N88-27162

AEROELASTIC CHARACTERISTICS OF THE AH-64 BEARINGLESS TAIL ROTOR

D. Banerjee
Chief, Aeromechanics R&D
Hughes Helicopters, Inc.
Culver City, CA 90230

Abstract

A Composite Flexbeam Tail Rotor (CFTR) with a structurally and aeroelastically unique hub design has been developed at Hughes Helicopters, Inc. (HHI) for the AH-64, Advanced Attack Helicopter. The full scale rotor has been successfully tested in the wind tunnel over the full steady sideslip envelope of the AH-64. The test program has defined the performance, loads, and dynamic characteristics of the CFTR for rotor speeds up to 1.0 N_R and airspeeds up to 197 knots. Uniqueness of the design is reflected in its patented hub design. The elastomeric shear attachment of the flexbeam to the hub results in a soft-inplane S-mode and a stiff-inplane C-mode configuration. The properties of the elastomer have been chosen for proper frequency placement and stable damping of the inplane S-mode. Both frequencies are well separated from the 1-flap frequency. The stress-critical pitch case/blade interface has been carefully designed to minimize loads. The flexbeam spanwise thickness and width distribution have been tailored for near-uniform corner stresses. The 1/rev chordwise load is maintained within the flexbeam and is not transferred to the hub. The 2/rev chordwise loads are transferred to the hub after significant attenuation due to hub shear pad damping and separation of the reactionless 1-chord frequency from 2/rev. The carry-through design of the flexbeam across the rotor hub allows the flexbeam to deform within the hub to reduce the hub loads to a minimum. Kinematic pitch-lag coupling is introduced to improve the first cyclic inplane C-mode damping at high collective pitch.

Presented at the Integrated Technology Rotor (ITR) Methodology Workshop, NASA Ames Research Center, Moffett Field, CA, June 20-21, 1983.

1.0 Introduction

Hughes Helicopters, Inc. (HHI) has designed, fabricated and successfully wind tunnel tested a Composite Flexbeam Tail Rotor (CFTR) for the AH-64 Advanced Attack Helicopter.

Over the past several years, a variety of bearingless tail rotors have been developed. The CFTR is a bearingless rotor whose design features have benefited from recent advances in composites technology and lessons learned from research into the basic characteristics of bearingless rotors that have to be addressed to achieve a successful design. Reference 1 describes the experimental development of a bearingless rotor and shows that a rotor system whose coupling effects are not well understood can run into fundamental dynamic instability problems. Instabilities encountered in the design were:

1) Inplane C-mode instability.
2) Inplane S-mode instability.
3) Stall flutter in the third flexible mode (torsion).
4) Stall flutter in the fourth flexible mode (second flap).

This reference also provides valuable information on the effect of key parameters such as blade sweep, tip weight, kinematic pitch-flap coupling, flexbeam width, etc., on the dynamic and aeroelastic behavior of the rotor. The choice of flexbeam geometry was found to be crucial to the level of flexbeam loads, and hence, the permissible amount of the kinematic pitch-flap coupling, which influences the flexbeam fatigue loads. In Reference 2, a hingeless rotor had a carefully designed flexbeam and was inherently stable. A closer look at this concept raised several questions regarding the "optimality" of the load path in the rotor. In Reference 3, the

rotor system encountered an instability involving the first flap/chord mode at moderate collective pitch. The rotor described in Reference 4 encountered flap-lag frequency coalescence and resultant instability which was eliminated by changing the pitch-flap coupling (δ_3) from a conventional value of -35 to -45 degrees (flap up induces pitch down), to +35 degrees, thus reducing the first flap frequency to below 1/rev. However care had to be exercised in the use of such pitch/flap coupling since it can lead to static divergence in flap/pitch. The rotor loads and performance characteristics resulting from the varying δ_3 were not addressed.

These rotors can be generally categorized as stiff-inplane or soft-inplane rotors. Typical problems associated with stiff-inplane rotors have been:

1) Inadequate structural stiffness in the flexbeam to ensure adequate separation of 1-chord and 1-flap frequencies. This generally results in coupled flap-lag instability (Reference 1).

2) Since the hub and drive system torsional stiffness lower the frequency of the 1-chord reactionless and collective modes, they have to be taken into account in sizing the flexbeam chordwise stiffness characteristics to avoid coalescence of the 1-chord and 1-flap modes.

3) In ensuring good separation of the 1-chord and 1-flap modes, the 1-chord frequency is generally placed high (between 1.5/rev and 1.7/rev). Dynamic amplification of 1/rev and 2/rev Coriolis bending moments result in high 1/rev and 2/rev chordwise fatigue loads in the flexbeam.

4) In order to accommodate the high loads of a stiff inplane rotor, a relatively stiffer flexbeam is required. This also increases the torsional stiffness of the flexbeam resulting in higher torsional loads on the control system.

Soft-inplane rotors have potential problems of:

1) Dynamic coupling of the rotor and support structure resulting in "ground resonance" type problems.

2) Structural loads in the flexbeam of a bearingless rotor could determine a lower bound on the flexbeam stiffness, and hence, the 1-chord frequency of the rotor blade.

With the above concerns in mind, the Composite Flexbeam Tail Rotor (CFTR) has been developed at Hughes Helicopters, Inc. It has a structurally tailored flexbeam chordwise stiffness distribution to locate the cyclic 1-chord frequency above 1/rev, and the flexbeam is mounted to the hub between elastomeric "soft" supports whose stiffness and damping are tailored to locate the collective and reactionless 1-chord frequencies below 1/rev. A description of the rotor design and dynamic characteristics are presented in Sections 2 and 3, respectively.

2.0 CFTR - Description

An exploded view of the CFTR is shown in Fig. 1. This shows that the axes of the blade-pair assembly are perpendicular to each other, and are separated axially so one flexbeam may cross over the other. The CFTR has upper and lower hub plates which sandwich the blade-pair assembly. The hub assembly is bolted to the tail rotor drive shaft. The flexbeam extends from the tip of one blade, across the hub, to the tip of the opposite blade. Bending and twisting motion of the flexbeam, between the edge of the hub and the inboard end of the blade, provides the fundamental flap, lag, and torsional motions of the rotor blades. The flexbeams are attached to the hub plates through elastomeric shear (inplane) pads. The laminated elastomeric pitch shear support aligns the pitch case with respect to the flexbeam. The pitch horn is bolted to the trailing edge of the pitch case. The spanwise location of the pitch link attachment is adjusted for an effective pitch-flap coupling (δ_3) of -35 degrees (pitch down with flap up). The pitch link is inclined to provide negative pitch-lag coupling (δ_4 positive: pitch up with blade lag) to augment inplane damping at high collective pitch and rotor speed. A brief description of each component follows.

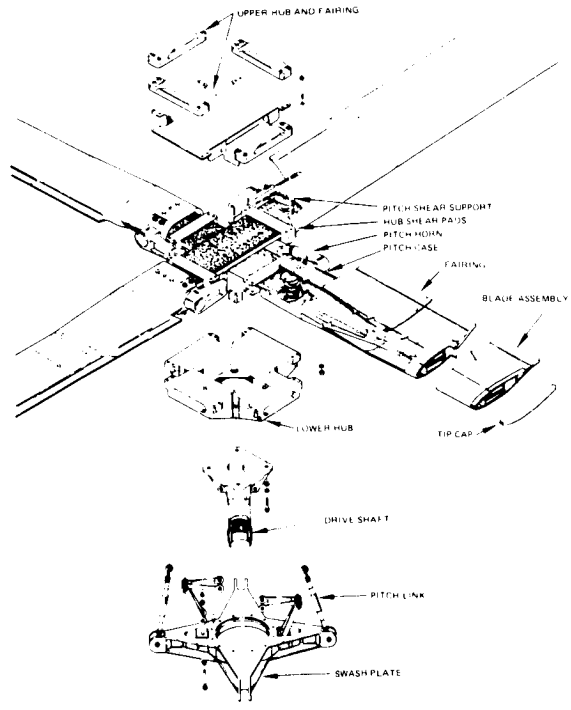

Fig. 1 CFTR assembly

2.1 Flexbeam

The heart of the CFTR is the fiberglass/epoxy flexbeam that carries across the full span of each blade-pair assembly and attaches the two blade sections of each blade-pair assembly to each other and to the hub. The flexbeam, which is of rectangular cross-section is built of layers of S-glass/epoxy with the filaments oriented ±5 degrees to the spanwise axis. S-glass was selected for its good fatigue strength, relatively high elongation, and low modulus of elasticity. Fiber orientation of ±5 degrees was selected as having a good fatigue strength and low torsional stiffness combined with the inplane shear strength to carry the driving torque and inplane blade loads. The spanwise distribution of flexbeam width and thickness is configured for near uniform spanwise distribution of combined corner stresses while maintaining a low structural torsional stiffness.

The flexbeam is formed as a flat beam that operates in the untwisted condition when the blade is producing design lift at $\theta_{3/4}$ = 8 degrees so that the torsional stress within the flexbeam is minimized.

2.2 Hub

The hub, as shown in Figs. 1 and 2, consists of upper and lower hub plates which sandwich the flexbeams between elastomeric inplane shear pads. Each set of pads is clamped between two load carrying beamlike structures; an upper hub plate "cross beam" and the "cross beam" stiffener of the lower hub plate. These beams carry shear loads due to preloading and reaction loading of the pads to support points on their ends. The pads themselves consist of an elastomeric section bonded to a thin aluminum plate which in turn is bonded to the flexbeam. Four anchor bolts (two on each end of each shear pad) attach the pads to the lower hub plate which carries all the reaction loads to the drive shaft. The elastomeric pads provide a soft mount between the flexbeam and hub and are designed to allow the flexbeam to bend with respect to the rigid hub and to keep the primary bending moments within the flexbeam where the filaments are oriented to accommodate them. In addition, the hub, which is of hollow construction, is designed to minimize the load path. These features are shown schematically in Fig. 3.

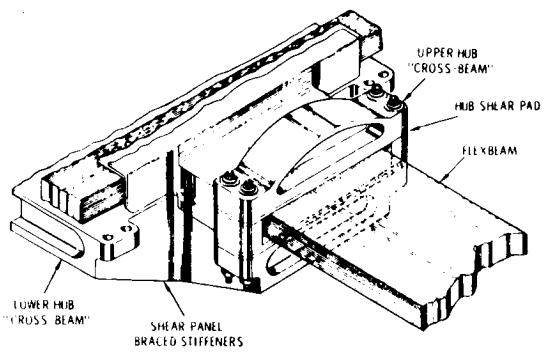

Fig. 2 Hub design

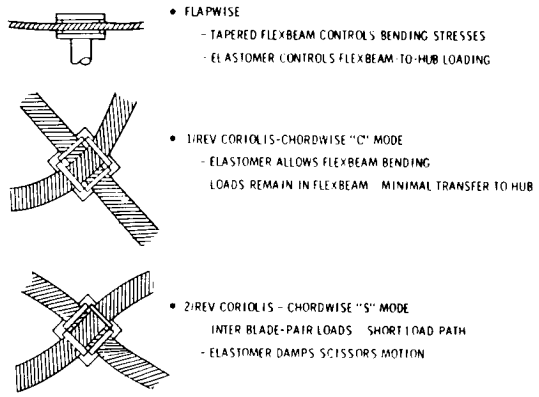

Fig. 3 Hub design criteria

In the flapwise direction, the flexbeam is designed for transfer of minimal bending moment loads into the hub as a result of the flexbeam taper and bending within the hub. The elastomer is clamped to preload it and ensure that it always has a net compression load. All flap bending loads are transferred between the flexbeam and hub through compression in the elastomer. The loads are transmitted by the upper hub plate "cross beam" and the lower hub plate "cross beam" stiffeners to the shear panel braced stiffeners (Fig. 2). These stiffeners are very deep and, therefore, are structurally very efficient for carrying the loads. The bolts for attaching the shaft flange to the lower hub plate are anchored at the intersection of these stiffeners with the central pocket. This results in the shortest possible load path.

Three predominant chordwise loads are encountered. The first is the steady driving torque which is reacted by the elastomer in shear. The other two result from Coriolis forces. The hollow hub allows the 1/rev Coriolis bending moment loads to be carried in the flexbeam instead of being transferred into the hub. The 2-rev Coriolis moments result in the inplane scissors S-type motion in which the adjacent blades work against each other as shown in the

lower sketch of Fig. 3. In this case, the loads are taken in shear through the elastomers and through short load paths across the rugged corners of the hub.

2.3 Pitch Case

The pitch case is a wet-filament wound fiberglass epoxy hollow structure that fits around, and is bonded to the flexbeam and blade root where these three components intersect. Inboard of the blade root, the pitch case enlarges to give the flexbeam room in which to twist as the blade feathers (Fig. 4). The pitch case tapers in the spanwise direction (Fig. 4) to reduce the flapwise stiffness (without sacrificing torsional rigidity). This minimizes the bending moment in the pitch case/blade root attachment induced by the pitch shear support and, hence, the resultant bending stresses. Near the inboard end of the pitch case, a hoop-wound stiffening ring provides the strength required to support the pitch horn and the elastomeric shear support loads.

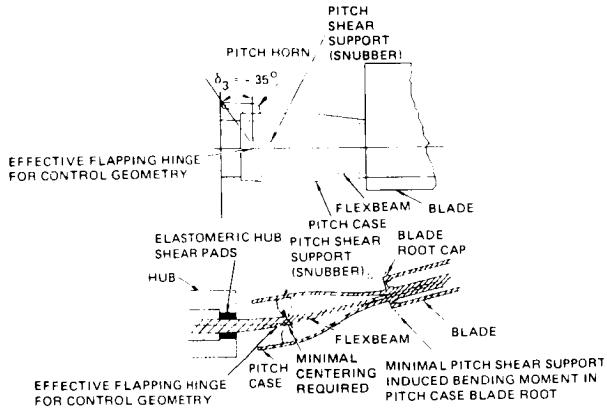

Fig. 4 CFTR blade root geometry

2.4 Pitch Shear Support ("Snubber")

The elastomeric pitch shear support is a laminated metal/elastomer device that is stiff with respect to radial loading, but soft in torsion and inplane shear. It centers the pitch case with respect to the flexbeam. Its spanwise location is kept well outboard, beyond the region of maximum flap bending curvature in the flexbeam. This minimizes the rotational deflection of the pitch case relative to the flexbeam as seen in the lower view of Fig. 4, and so minimizes pitch shear support-induced bending moments at the point where the pitch case, flexbeam, and blade join at the blade root station.

2.5 Blade

The primary material for the wet filament wound blade structure is Kevlar-49/epoxy.

Unidirectional fibers with maximum tensile strength and modulus are used for leading edge obstacle strike protection, and for the trailing edge longo that carries high axial loads and has high stiffness. The airfoil-shaped blade section is a multi-tubular Kevlar/epoxy structure that is bonded around the flexbeam (Fig. 5). A C-shaped channel is added in the aft airfoil region to stiffen the outer skin. The leading edge balance weight is a multiple-rod molded construction. The small diameter rods easily conform to twisted contour of the leading edge. The portion of the leading edge cavity between the leading edge balance weight and Kevlar spar tubes is filled with syntactic foam.

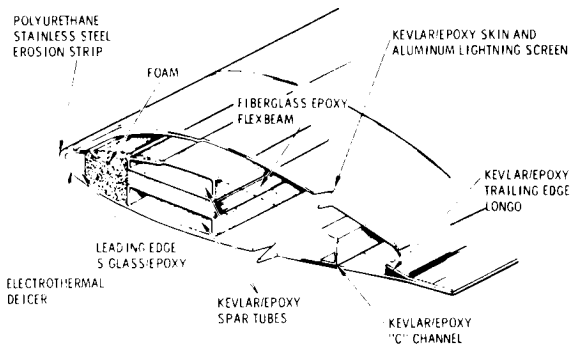

Fig. 5 CFTR blade cross-section

The blade has a -9 degree twist, and is positioned about the flexbeam so that when the flexbeam is untwisted, the blade pitch angle at 3/4-radius is 8 degrees. The orientation of the flexbeam with respect to the blade chord at different radial stations is shown in Fig. 6.

3.0 CFTR - Dynamics

The fundamental mode of instability for bearingless rotors has been shown both analytically and experimentally to be associated with the coupling between the first flap and the first inplane (reactionless and cyclic) modes (References 1, 3, 4, 5, 6 and 7). For bearingless tail rotor designs (References 1, 2 and 4), the inplane frequency generally lies between 1 and 2/rev, with the reactionless (S) mode frequency slightly

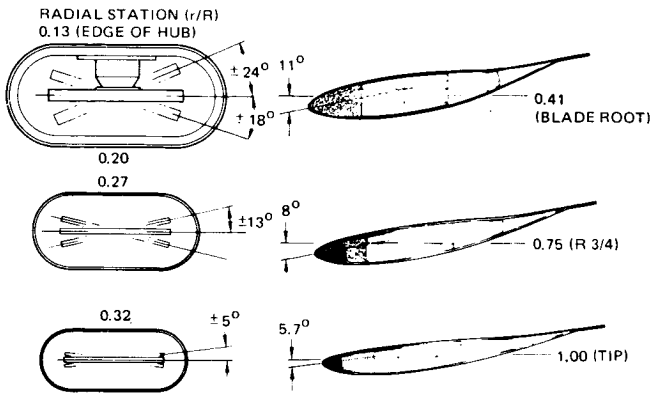

Fig. 6 Blade/pitch case/flexbeam cross-sections

lower than the cyclic (C) mode frequency - the difference depending on the hub configuration and the rotor pylon structural properties. Both an increase in collective pitch and (conventional) negative pitch flap coupling tend to bring the first flap and the first inplane frequencies closer together, by increasing the first flap frequency and lowering the first inplane frequency. This often results in the lightly damped first inplane modes (both the reactionless and cyclic) becoming unstable. Typical solutions to the above problem have been the stiffening of the flexbeam in the chordwise direction (Reference 1) and the use of positive pitch flap coupling (References 4 and 6) to separate the modes. These solutions have been applied with limited success because first, structural design considerations put a limit on the chordwise stiffness of the flexbeam, and second, even though a stable rotor system was presented in Reference 4 (with positive pitch-flap coupling), similar experimental effort in Reference 1 showed the presence of a stall-induced flap-lag-torsion large amplitude limit cycle instability.

At HHI, the above dynamic problems have been solved for the CFTR by lowering the S-mode inplane frequency below 1/rev (soft inplane) while maintaining the C-mode inplane frequency above 1/rev (stiff inplane) and well separated from the first flap frequency. Some of the design parameters that resulted in this dynamically unique bearingless tail rotor design are discussed below.

3.1 Flexbeam to Hub Support

By supporting the flexbeam to the hub through elastomeric hub shear pads with no restraint within the hub, the S-mode inplane shear and bending moments are reacted through the elastomeric hub shear pad. The stiffness of the shear pad has been tuned to accurately place the first S-inplane frequency below 1/rev (this frequency for the current design is at approximately 0.6/rev) and well separated from the first flap frequency at all operating conditions. The damping in the shear pad elastomer provides a high level of damping in the first S-inplane motion. This, along with its large separation from the 2/rev resonance condition ensures a low level of blade dynamic loading for the 2/rev Coriolis forces. In the C-mode inplane configuration, the hollow construction of the hub and the influence of the elastomeric shear pads allows the flexbeam to bend within the hub. This ensures that the bending moment loads are carried across the hub within the flexbeam. Since the inplane loads are not reacted by the shear pads in this configuration, the first C-inplane frequency stays well above 1/rev. The location of this frequency and its damping can be optimized by proper choice of flexbeam width, tip weight, pitch-flap coupling and other parameters.

3.2 Flexbeam Geometry

A rectangular flexbeam configuration was chosen. However, the spanwise distribution of width and thickness were tailored for optimum placement of fundamental 1-flap and 1-chord frequencies as well as acceptable combined corner stresses. The "soft" hub mount of the flexbeam and root-end kinematic pitch-lag coupling ensured high damping of the rotor chord modes. Hence no attempt was made to sandwich elastomeric material into the flexbeam design. The chordwise stiffness was designed for adequate separation of 1-chord and 1-flap frequencies. The spanwise distribution of flexbeam width and thickness has been configured for near uniform spanwise distribution of combined corner stresses while maintaining a low structural torsional stiffness. This is vitally important as can be seen in Fig. 7, which shows a comparison of flapwise bending stresses for different flexbeam configurations for a blade flapping of $\beta = 15$ degrees. Detailed calculations show that a flexbeam with a uniform width and thickness is totally unacceptable for fatigue loads at high forward speeds.

3.3 Tip Weight

The tip balance weight has been eliminated for the CFTR. This results in a simpler tip design without a tip weight attachment fitting. Since the fundamental dynamic effect is an increased first C-mode chordwise frequency, the removal of the tip weight is beneficial in separating the first flap and the first chord frequencies. The spanwise balance weight is located on the top and bottom of the pitch case at its root end (Station 10.0). This location results in reduced

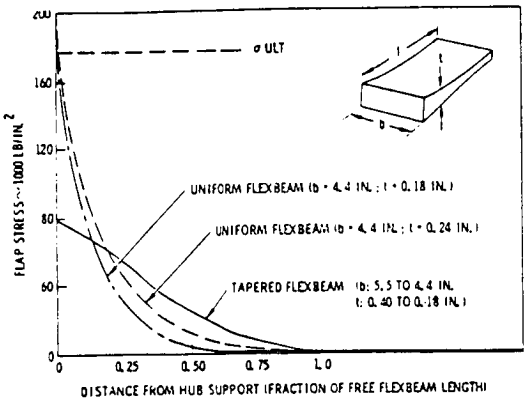

Fig. 7 Flapwise flexbeam stress (blade flap = 15 degrees)

feathering control loads due to reduced "tennis racquet" effect.

3.4 Pitch Link Attachment

The pitch link is attached to the trailing edge of the pitch case. For the design value of negative pitch-flap coupling (δ_3 = -35 degrees), the blade spanwise pitch horn attachment point is well inboard, resulting in a small swashplate and a compact design. In addition, the direction of the pitch link load is the same as that of the rotor thrust, thus reducing the flexbeam flap shear load. Dynamically, because of the inboard attachment of a trailing edge pitch link, the second flap frequency is much higher than it would be for a leading edge attachment. This is very important in raising the second flap frequency above and maintaining good separation from 3/rev. As shown in Fig. 1, the pitch link is inclined radially inwards from the swashplate to the pitch horn at an angle of 70 degrees to the hub plane. This induces kinematic pitch-flap-lag coupling to improve the first inplane (C-mode) damping at high collective pitch settings. The coupling results in positive pitch-lag motion, i.e., nose down with blade lag motion. This is in general agreement with the requirement for stiff-inplane rotors.

3.5 Chordwise Blade Balance

As in the existing AH-64 metal tail rotor the chordwise c.g. of the CFTR blade has been located at 35 percent chord to reduce the weight of the blade and the "tennis racquet" loads on the control system. Ballistic damage considerations, however, require the rotor to be stable with a failed pitch link. This condition is satisfied by stabilizing the coupled pitch-flap mode with a leading edge weight in the outboard portion of the blade between 70 and 90 percent radius.

4.0 Wind Tunnel Test Procedure

4.1 General Description

The Composite Flexbeam Tail Rotor (CFTR) was evaluated through extensive wind tunnel tests to determine rotor performance, loads, and dynamic characteristics in hover and in low and high speed forward flight, and in sideslip conditions that are representative of the production AH-64 flight spectrum.

Testing was conducted in the Boeing Vertol V/STOL wind tunnel located at Philadelphia, Pennsylvania. The essential objectives of the wind tunnel tests were:

1) Define dynamic and aeroelastic stability characteristics of the CFTR over the sideslip flight envelope of the AH-64.
2) Define rotor loads, and blade load and stress characteristics.
3) Define performance characteristics.
4) Define start/stop response characteristics.

A fully instrumented blade pair assembly was mounted on the Dynamic Rotor Test Stand (DRTS). The DRTS assembly provided support, control, and drive for the CFTR. A typical installation with the rotor positioned for forward flight with sideslip is shown in Fig. 8. Sideslip was simulated by presetting the sting inclination, and remotely controlling the DRTS pitch angle. Twenty-six rotating gages were monitored. This included flap, lag and torsion gages on the flexbeam and the blade, pitch link, rotor hub, output shaft, etc. Additional rotating and non-rotating measurements include shaft torque balance thrust, pitching and rolling moments, shaft angle, RPM indicator, control system load, etc.

4.2 Control System and Rotor Support System

A close-up view of the drive and support system is seen in Fig. 9. The test stand drive shaft is coupled to the output drive shaft of the rotor with adapting hardware. The "scissors" drive the rotating swashplate from the output shaft.

The control system consists of the pitch link attached to the pitch horn at one end and to the rotating swashplate at the other. The non-rotating swashplate is mounted on two hydraulic actuators (Fig. 9) spaced apart azimuthally by 180 degrees.

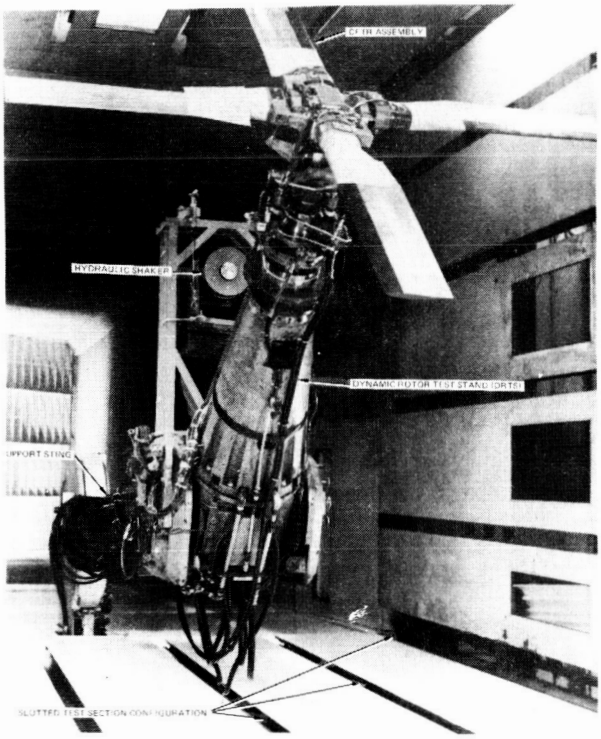

Fig. 8 Composite flexbeam tail rotor in the wind tunnel test section

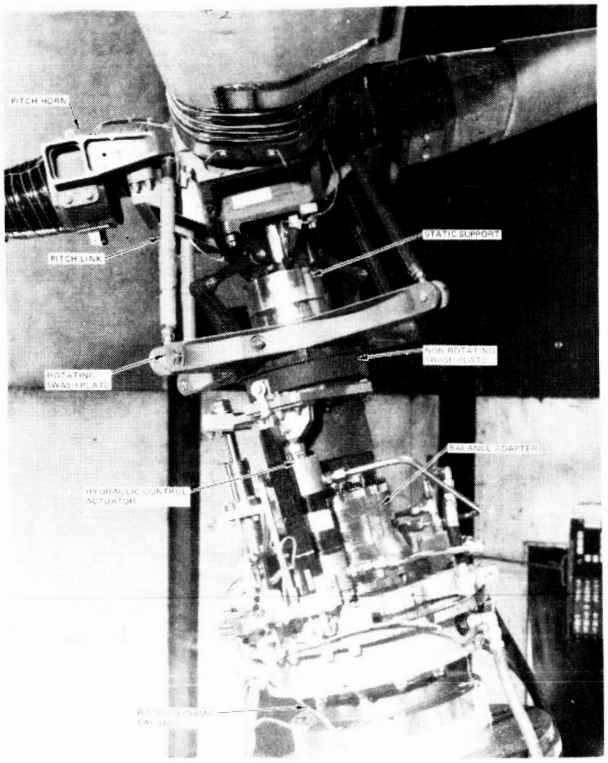

Fig. 9 CFTR drive and support system assembly

The static mast is mounted on the DRTS with an interface hardware called the balance adapter that is in turn supported to the test stand with a dynamic balance. The dynamic balance (Fig. 9) is strain-gaged to measure the CFTR thrust, rolling and pitching moments.

A description of the test rotor components is provided in Reference 9.

4.3 Collective and Cyclic Excitation

In preparation for wind tunnel tests, provision was made to excite the rotor using collective and cyclic shakers. These were available to excite lowly damped fundamental rotor modes in order to measure their damping characteristics.

Cyclic modes were driven by a 300 lbf, 0-200 Hz, shaker mounted on the sting as shown in Fig. 8. The shaker excitation was applied to the Dynamic Rotor Test Stand (DRTS) below the stand balance.

Collective excitation was provided through the collective pitch hydraulic drive system. The collective pitch excitation was used with an amplitude of ±0.5 degree blade pitch change over a frequency range 0 - 35 Hz.

4.4 Test Precautions

Procedures that were established to ensure the integrity of the CFTR through the complete test envelope included:

Non-rotating rap tests were done at the start of each day's testing. The response of the blade in the flap, lag and torsion degrees of freedom were observed on the spectrum analyzer. In addition to visual inspection, this test provided confidence in the structural integrity of the CFTR.

Selected rotor response gages were continuously monitored for all test conditions on twelve on-line monitors and the spectrum analyzer. Certain critical gages, in addition to performance parameters, were also observed on the on-line flatbed plotters.

Additional test protection was observed by introducing the collective pitch dump capability that was designed to automatically drop the collective pitch to a previously tested safe level when any one of selected critical gage response exceeded a prespecified value. Spectral analyzers were also used to continuously monitor the non-harmonic content of selected responses.

This procedure for on-line data monitoring and automatic collective pitch dump, safety of the CFTR wind tunnel test was assured.

4.5 Test Stand Shake Test

Prior to mounting the CFTR on the Dynamic Rotor Test Stand (DRTS), a shake test was conducted to determine dynamic characteristics of the test stand. The purpose of this investigation was to:

1) Identify and isolate CFTR response characteristics that were essentially the influence of test stand dynamics.

2) Determine any distabilizing influence of the test stand on the rotor dynamics.

This was done by determining the test stand frequencies, generalized masses, generalized dampings, and mode shapes of all modes in the frequency range 0 - 100 Hz. The hub modal data was incorporated in a fully coupled CFTR/DRTS aeroelastic stability analysis to verify that the integrated systems are free from adverse dynamic or aeroelastic coupling.

The influence of the test stand on the CFTR modal characteristics were found not to be significant.

4.6 Data Reduction Facility

Test data was processed for on-line or off-line reduction and presentation. Off-line digitized data was available in four formats.

1) Low Speed Calculated Data presents steady state static data of wind tunnel test configuration. This data includes rotor advance ratio, RPM, shaft angle, collective pitch, C_T, C_p, velocity of wind tunnel, balance steady thrust pitching and rolling moments, velocity of sound, etc.

2) High Speed Calculated Data essentially calculates the steady and alternating values of the different interaction equations (combined stresses).

3) Stress Analysis Data presents the steady and alternating values of 29 channels of data being monitored for each test point.

4) Harmonic Analysis Data presents the magnitude and phase of the first 10 harmonics of all 29 channels of data recorded.

Six on-line flatbed plotters were used to plot any combination of dimensional or nondimensional parameters in their final corrected forms. Also available was on-line spectral analysis of any selected data channel and corresponding hard copies.

The wind tunnel control console offered on-line monitoring of many key control parameters. These were viewed in alphanumeric or analog form on digital displays, oscilloscopes, or oscillographs. A safety-of-flight monitor was also provided. This data was continuously recorded from a number of preselected data channels whenever the rotor or tunnel was activated. The parameters that triggered the rotor blade pitch dump were monitored in analog form on oscilloscopes.

5.0 Evaluation of Results

The test program determined the performance, loads, and dynamic characteristics of the CFTR for rotor speeds up to 1.0 N_R and airspeeds up to 197 knots. The complete impressed pitch range, as limited by test stand capabilities or rotor structural requirements was investigated in hover, low and high speed forward flight and sideslip conditions. Static sideslip limits as defined in the AH-64 System Specification (Reference 10) were investigated at airspeeds of 139, 164, and 197 knots. The stop/start characteristics of the rotor in wind velocities up to 45 knots were defined. The test explored the full steady state sideslip envelope of the AH-64 as seen in Fig. 10 where test points are superimposed on the helicopters sideslip envelope.

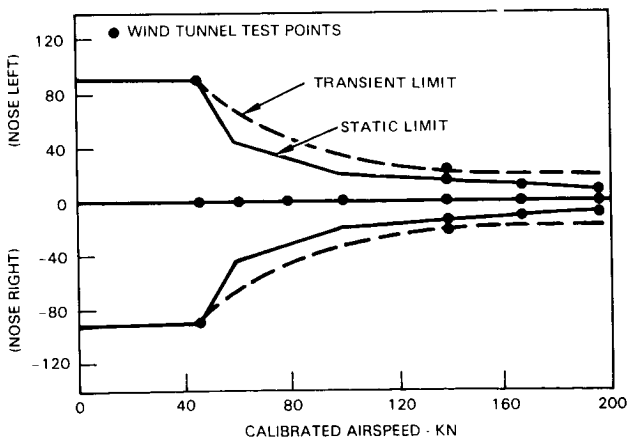

Fig. 10 AH-64A sideslip envelope

For hover tests, the rotor speed was varied from 0 to 1.0 N_R (1403 RPM) in steps of 0.2 N_R (420 RPM). Collective pitch was varied over the full range that was available at 0.8 N_R, 0.9 N_R and 1.0 N_R within the limits of the test stand capability.

Fig. 11 presents a comparison of the CFTR power versus thrust coefficient as measured in the wind tunnel at zero wind tunnel speed. Fig. 12 is the corresponding plot of rotor thrust coefficient versus impressed blade pitch setting.

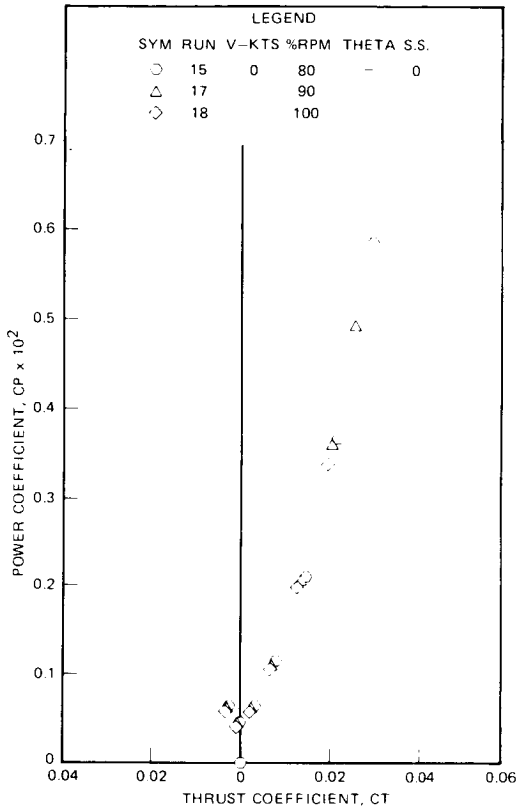

Fig. 11 Hover test, baseline blade performance data

Forward flight tests were conducted for the conditions shown in Fig. 10. Sideslip angles at V = 138 knots, 164 knots and 197 knots were essentially restricted to the steady sideslip limits. Attempts to test at higher left and right sideslip angles resulted in autorotation of the rotor for zero collective pitch. This, of course, is a test stand limitation and will not be encountered in actual flight.

Typical spanwise distribution of flexbeam and blade loads at V = 164 knots and β_{SS} = +6 degrees is shown in Figs. 13 through 18. Pitch case loads (station 4.2 to 25.0 inches) are not shown in these figures since it was not instrumented. Flexbeam loads for various pitch angles are shown between station 6.2 inches and 25.0 inches and the blade loads between station 25.0 inches and 56.0 inches. The pitch case,

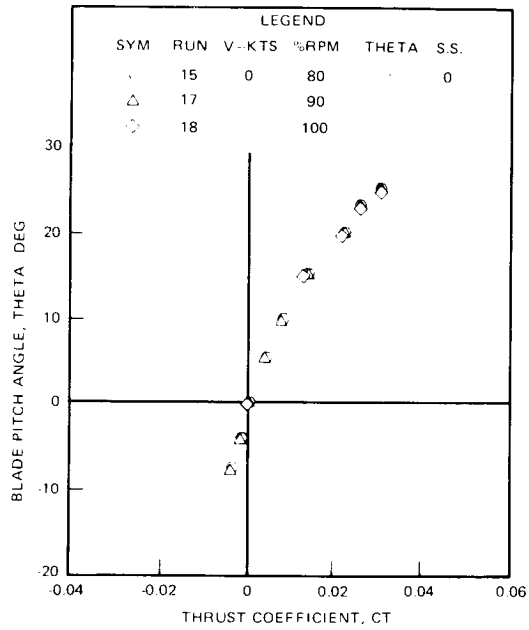

Fig. 12 Hover test, baseline blade performance data

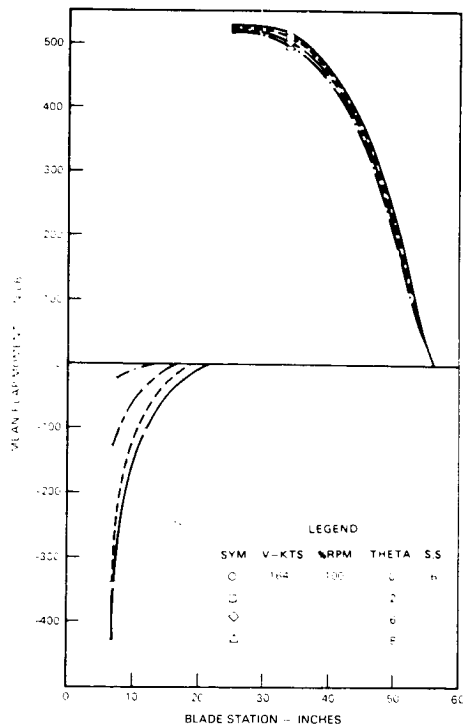

Fig. 13. CFTR wind tunnel test - mean flap moment distribution

flexbeam, and blade junction is at station 25.0. These stations are important in understanding the discontinuities and inflections in the bending moment plots.

The steady loads between the pitch case, flexbeam and blade should balance at the junction, station 25.0. However, because of phase differences between the loads in the pitch case, flexbeam, and blade, the plots of the oscillatory loads do not necessarily add up at the junction.

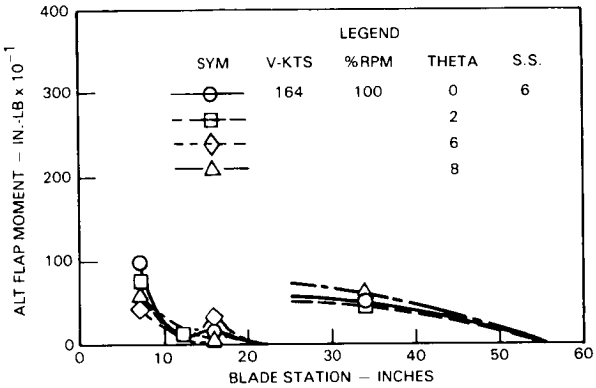

Fig. 14 CFTR wind tunnel test - alternating flap moment distribution

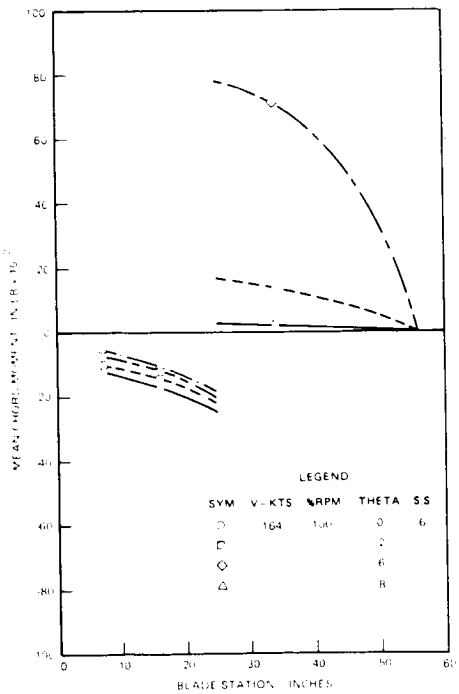

Fig. 15 CFTR wind tunnel test - mean chord moment distribution

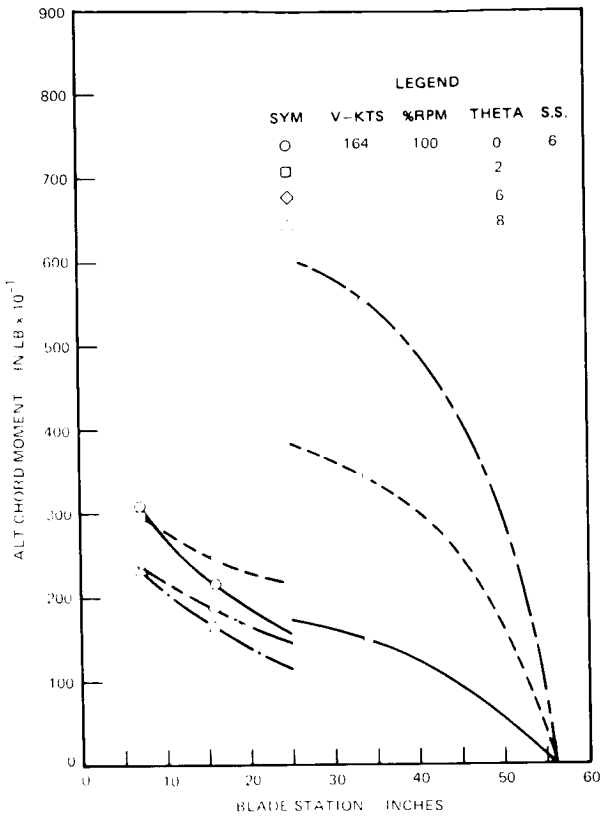

Fig. 16 CFTR wind tunnel test - alternating chord moment distribution

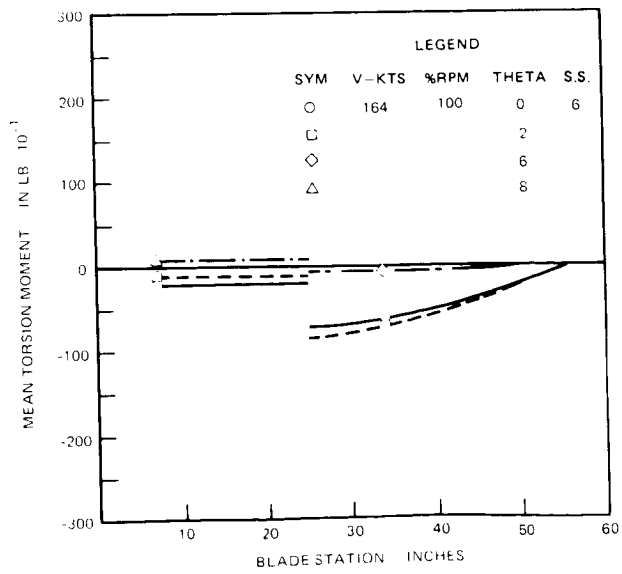

Fig. 17 CFTR wind tunnel test - mean torsion moment distribution

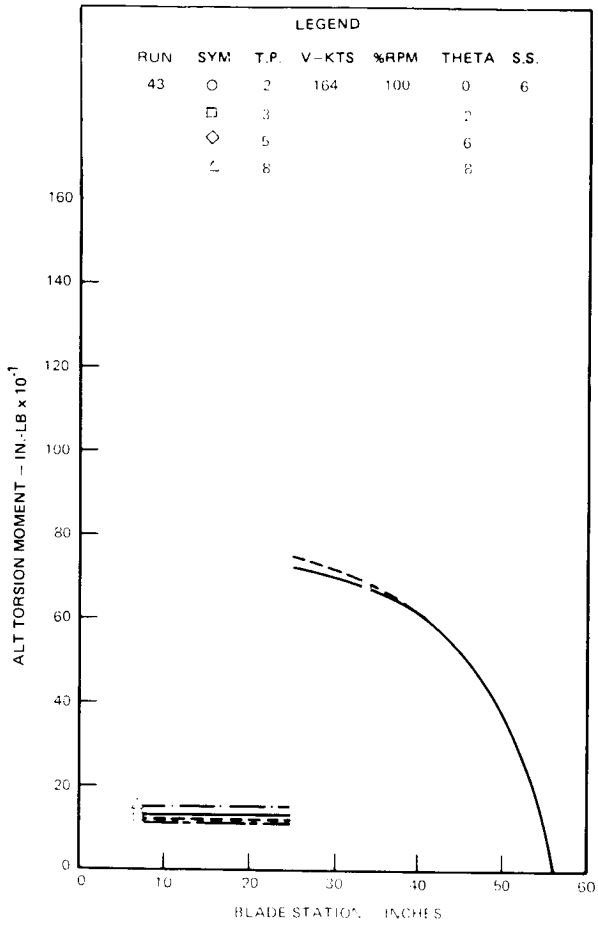

Fig. 18 CFTR wind tunnel test - alternating torsion moment distribution

Steady and alternating flapwise bending moments are shown in Figs. 13 and 14. Both show a steep drop in flexbeam bending moment from the edge of the hub to approximately station 10.0 inches. As per design, the flexbeam flap bending moment tapers to practically zero between station 20.0 inches and 25.0 inches. The jump discontinuity in the bending moment between the flexbeam and blade at station 25.0 is the bending moment in the pitch case. The flapwise bending moment in the pitch case would reduce to zero at the pitch link/pitch horn attachment. Similarly, the bending moment distribution is drawn such that the value at the blade tip (station 56.0 inches) is zero. Chordwise bending moments are seen in Figs. 15 and 16. The discontinuity at station 25.0 inches reflects the chordwise loads in the pitch case. The component of pitch link compression load in the chordwise direction produces this bending moment. The chordwise load in the pitch case is essentially the result of the pitch link inclination. Unlike the flap bending moment distribution, the chordwise moment in the flexbeam has a more gradual distribution. The torsion bending moments are shown in Figs. 17 and 18. The steady flexbeam torsion load is due to the steady wind-up of the flexbeam. Measured flexbeam torsional load for $\theta_{3/4} = 8$ degrees is approximately zero since the flexbeam is untwisted at this pitch setting. The difference between the blade and flexbeam torsion bending moment at station 25.0 inches is the torsion load in the pitch case reacted by the pitch link. Fig. 17 also shows the relative magnitude of the flexbeam torsion load to the pitch link load. Alternating torsion load in the flexbeam is a result of flexbeam feathering with blade flapping with the root-end pitch flap (δ_3) coupling.

5.1 Dynamic Results

As discussed in Section 4.3, collective and cyclic shakers were available to excite lowly damped fundamental rotor modes in order to measure their damping characteristics.

The collective pitch excitation had an amplitude of ±0.5 degrees blade pitch change over a frequency range of 0 - 35 Hz. The cyclic excitation was input as non-rotating test stand force with the 300 lbf shaker. Shaker forces of 50 lbf and 100 lbf were used from 0 - 70 Hz.

Accordingly, collective and cyclic excitation were attempted to excite the rotor modes at each point in hover in the test envelope. However, after many attempts it was determined that the rotor fundamental modes were heavily damped and, hence, could not be excited with either of the two shakers. It was decided at this point that envelope expansion of CFTR wind tunnel test would be based on the magnitude of non-harmonic flap, lag or torsion response as seen on the on-line spectrum analyzer.

Dynamic analysis research tool (DART) analysis program was used to define the CFTR dynamic and aeroelastic characteristics and blade loads of the CFTR. This program is described in Reference 11.

Two basic types of analysis were used to substantiate the dynamic and aeroelastic characteristics of the CFTR. First, an eigenvalue analysis was used for configurations in hover to establish freedom from aeroelastic instability throughout the complete blade pitch and rotor speed ranges of the CFTR. This also established the blade modal characteristics. Second, forward flight stability was established by trimming the rotor at

different points of the flight envelope. Since the analysis included nonlinear structural couplings and aerodynamics (including dynamic stall), rotor trim without nonharmonic response indicated positive stability margins.

The resonance diagrams generated by DART for reactionless, cyclic and collective boundary conditions are shown in Figs. 19, 20 and 21, respectively. Test frequencies obtained at zero and operating RPM are superimposed on the resonance diagrams.

Tabulated results of the non-rotating rap tests are shown in Table 1. The fundamental 1-flap, 2-flap, 1-chord and 1-torsion modes show good correlation with analytical data. Spectral plots of non-rotating rap tests for flexbeam chord and flap gages are shown in Figs. 22 and 23, respectively.

Results of cumulative spectrum plots for different forward flight tests are shown in Table 2. Spectral plots for one flexbeam chord gage for V = 139 knots and 197 knots are shown in Figs. 24 and 25, respectively.

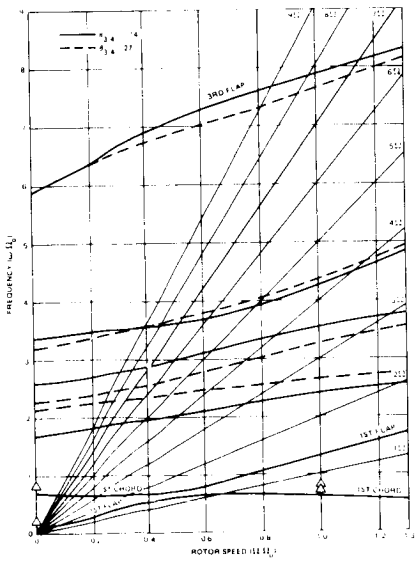

Fig. 19 CFTR resonance diagram - reactionless modes

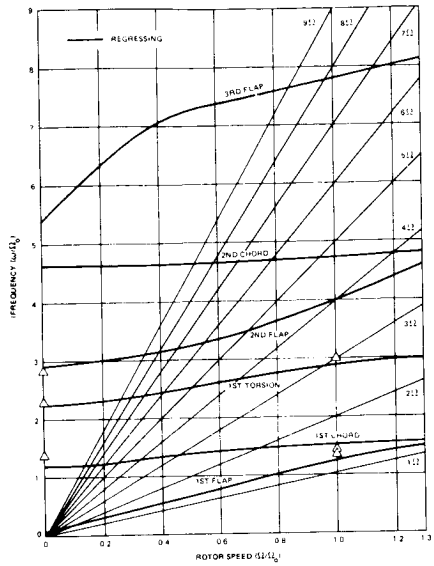

Fig. 20 CFTR resonance diagram - cyclic modes, $\theta_{3/4} = 0$

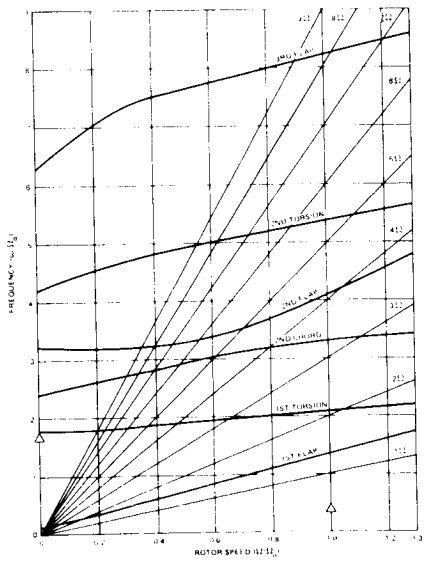

Fig. 21 CFTR resonance diagram - collective modes, $\theta_{3/4} = 0$

Table 1. Nonrotating Modal Frequencies - Correlation of Test Results with Analysis

Configuration	Mode	Frequency - Hz (/Rev) Analysis	Test
Reactionless Boundary Condition	1-Flap	3.5 (0.15)	4.4 (0.19)
	1-Chord	16.4 (0.7)	18.2 (0.78)
Cyclic Boundary Condition	1-Chord	30.4 (1.3)	32.3 (1.38)
	1-Torsion	51.4 (2.2)	53.8 (2.3)
	2-Flap	69.0 (2.95)	70.2,(3.0, 66.4 2.84)
Collective Boundary Condition	1-Torsion	40.9 (1.75)	40.0 (1.71)
	2-Flap	57.3 (2.45)	58.0 (2.48)

Table 2. Inplane Modal Frequencies for Various Test Conditions

Figure No.	Test Condition V(KTS)	β_{ss} (Deg.)	Collective Pitch	Flexbeam Chord Gage Resonant Frequencies Hz (/Rev)
–	25	-90	Sweep	8.4 (0.36/Rev); 17.8 (0.76 Rev); 33.0 (1.41 Rev)
24	139	+15	Sweep	6.8 (0.29/Rev); 16.8 (0.72/Rev); 29.0 (1.24/Rev); 70.0 (3/Rev)
25	197	-8	Sweep	7.5 (0.32/Rev); 15.2 (0.65/Rev); 29.7 (1.27/Rev); 70.0 (3/Rev)
–	197	-2	Sweep	7.5 (0.32/Rev); 15.7 (0.67/Rev); 29.5 (1.26/Rev); 70.0 (3/Rev)
–	0-164 Sweep	0	0	7.7 (0.33/Rev); 16.8 (0.72/Rev); 30.5 (1.30/Rev); 70.0 (3/Rev)

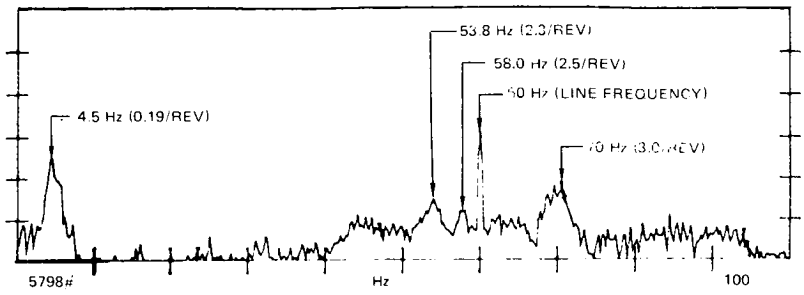

Fig. 22 Frequency spectrum of flap response - nonrotating rap test

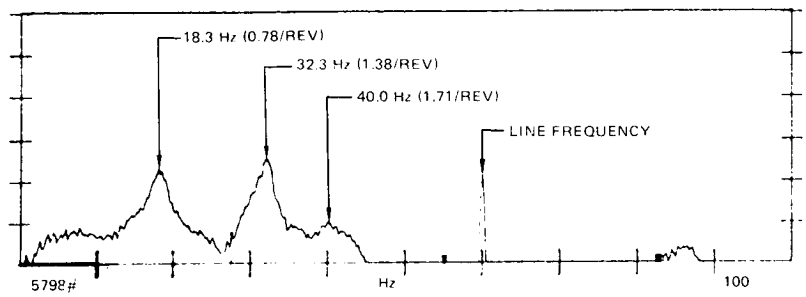

Fig. 23 Frequency spectrum of chord response - nonrotating rap test

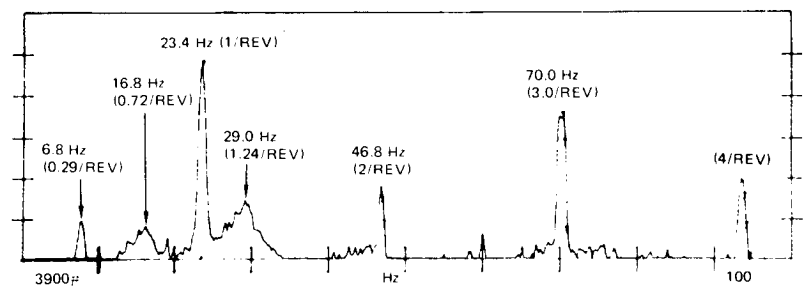

Fig. 24 Frequency spectrum of flexbeam chord response - V = 139 knots, β_{ss} = +15 degrees, θ sweep, Ω = 1403 rpm

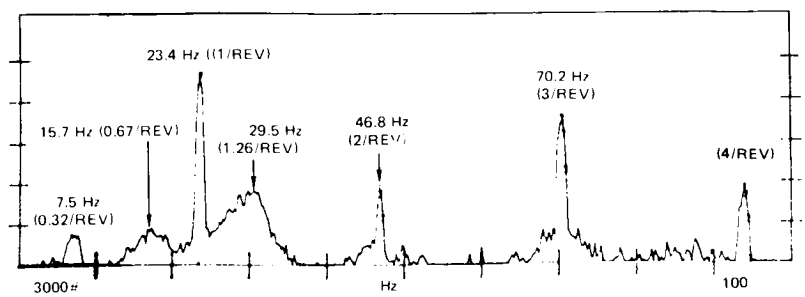

Fig. 25 Frequency spectrum of flexbeam chord response - V = 197 knots, β_{ss} = -8 degrees, θ sweep, Ω = 1403 rpm

5.1.1 Reactionless Boundary Condition

The reactionless boundary condition corresponds to an isolated rotor. The reactionless modes resonance diagram for the collective pitch extremes of -14 degrees and +27 degrees is shown in Fig. 19. In the reactionless or "scissors" (S-mode) inplane boundary condition, the steady and 2/rev inplane shear and bending moments are reacted through the elastomeric hub shear pads. The stiffness and damping of the shear pads provide the hub restraint for blade chordwise motion. The first chord frequency is primarily dependent on the stiffness and spanwise offset of the hub shear pad. Its frequency is located at approximately 0.6/rev which provides good separation from the first flap frequency and 2/rev Coriolis excitation. The first flap frequency is governed by the effective hinge offset (approximately 10 inches) and the value of kinematic pitch-flap coupling. The first flap is generally highly damped. The high damping of the first chord mode is a reflection of hub shear pad damping characteristics. This is evidenced by the results of shake tests using the collective and fixed system shakers. Since the hub shear pads do not feather with pitch change, the first chord frequency and damping remain essentially unchanged with change in blade collective pitch. The first flap frequency and damping are generally unchanged with collective pitch.

The higher modes have been shown analytically (Reference 11) to be well damped with minimal change with collective pitch.

The coupled mode shapes corresponding to the fundamental modes are shown in Figs. 26 and 27. The first chord mode, Fig. 26, shows very little coupling with the flap and torsion motion of the blade. The elastic deflection in the chordwise direction is essentially in the hub shear pad with the blade moving as a rigid body. The first flap mode, Fig. 27, shows the coupling between the blade flap and torsion motion (pitch/flap coupling).

In contrast to conventional rotors, the first torsion mode reflects feathering motion about the pitch link/pitch horn attachment. The shear stiffness of the snubber in flap and chord and the chordwise stiffness of flexbeam between station 15.0 inches and 25.0 inches, in addition to the control system stiffness, have significant influence on the frequency of this mode. This is determined from the strain energy data corresponding to the first torsion mode.

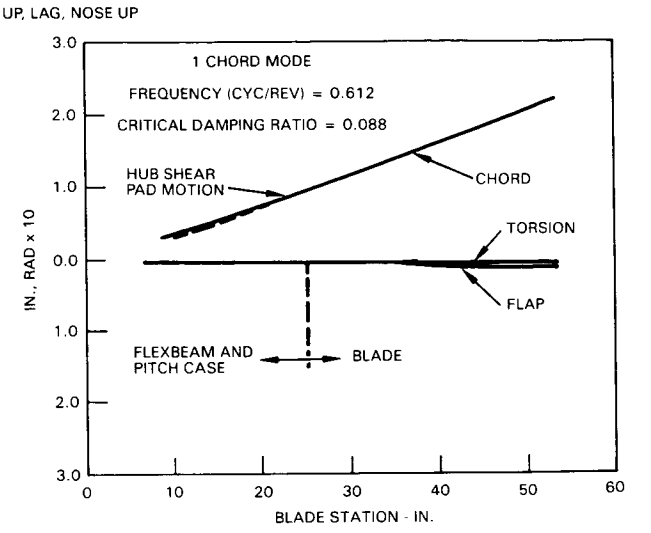

Fig. 26 Reactionless B.C., mode shape plots – 1-chord mode

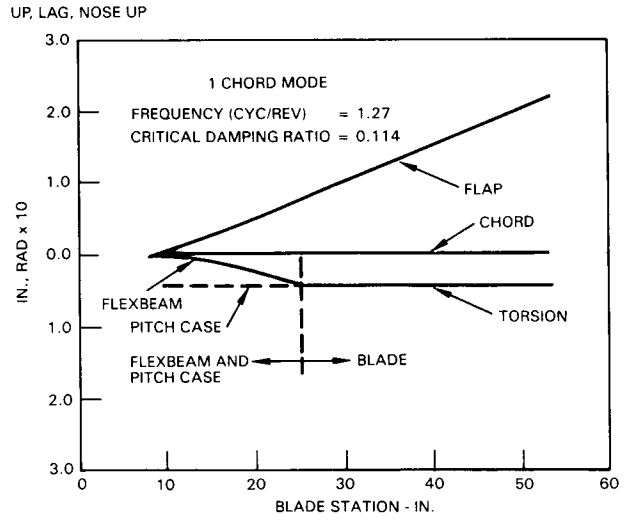

Fig. 27 Reactionless B.C., mode shape plots – 1-flap mode

5.1.2 Cyclic Boundary Condition

In the cyclic or C-mode boundary condition, the 1/rev inplane bending moments are contained within the flexbeam in the carry-through hub construction and are not reacted through the hub shear pads and the hub. The hub support flexibility is modeled. The coupling between the hub

motion and blade feathering due to swashplate motion is included. The kinematic flap-lag-torsion coupling due to pitch link/pitch horn spanwise and chordwise location and pitch link inclination is also included in the analysis.

The regressing frequencies for zero collective pitch are shown in Fig. 20. The first chord frequency, which reflects the stiffness of the flexbeam and the inertia of the blade, is well separated from the first flap frequency and from 1/rev resonance.

Fig. 28 shows the influence of collective pitch on blade frequencies. The first flap frequency remains practically unchanged with collective pitch. The pitch orientation of the flexbeam with respect to the blade chord ensures minimal variation of the first chord frequency over the collective pitch range of the rotor. The first torsion mode shows a drop in frequency with collective pitch thus further separating it from 3/rev. As expected, the second flap frequency increases and the second chord frequency decreases with changes in collective pitch from zero.

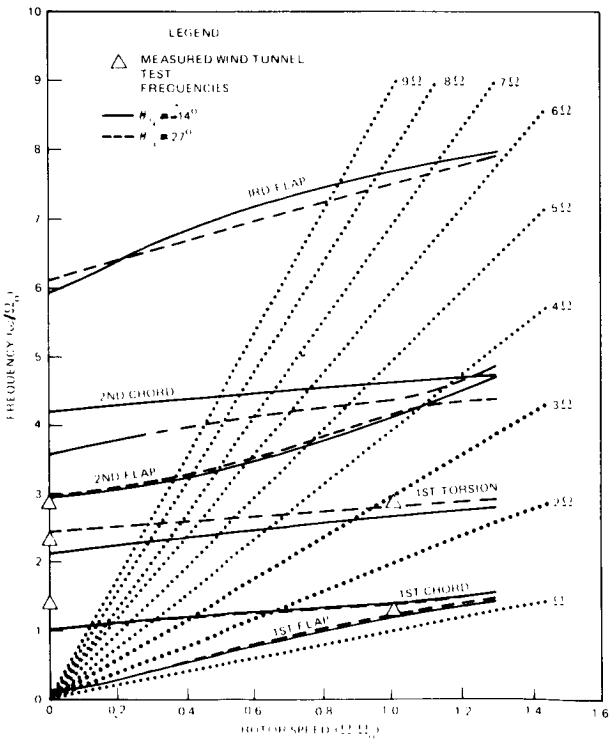

Fig. 28 CFTR resonance diagram; cyclic modes $\theta_{3/4}$ = -14 and 27 degrees

Figs. 29 through 31 show the fundamental coupled mode shapes for the cyclic boundary condition. The first flap mode, Fig. 29, shows the pitch/flap coupling for cyclic boundary condition. The first chord mode shows the amount of kinematic pitch/lag coupling induced by the inclined pitch link. The first torsion mode, Fig. 31, shows the extent of flap coupling.

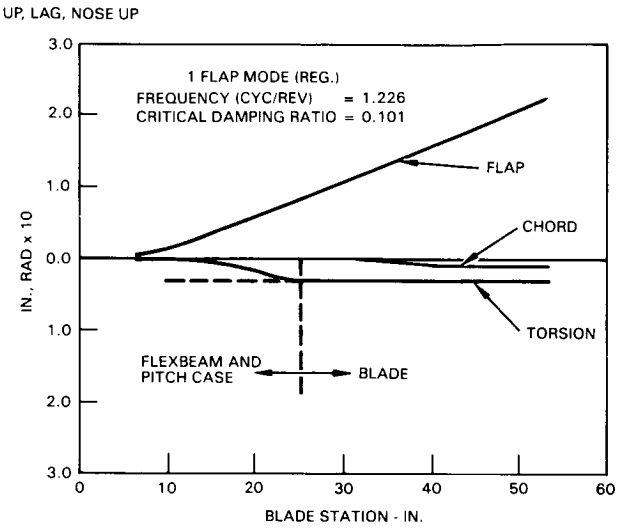

Fig. 29 Cyclic B.C., mode shape plots – 1-flap mode

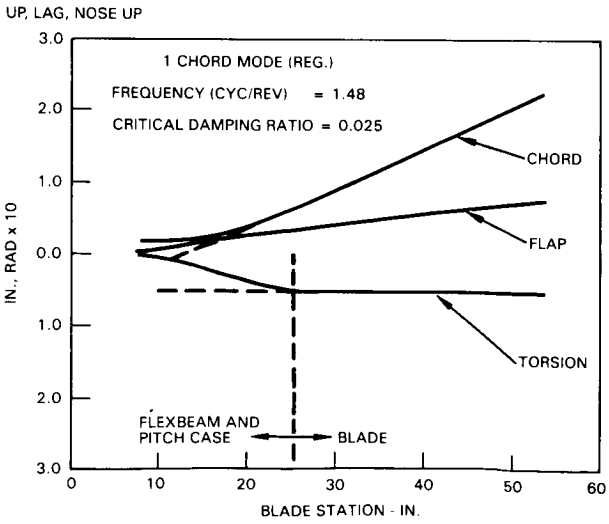

Fig. 30 Cyclic B.C., mode shape plots – 1-chord mode

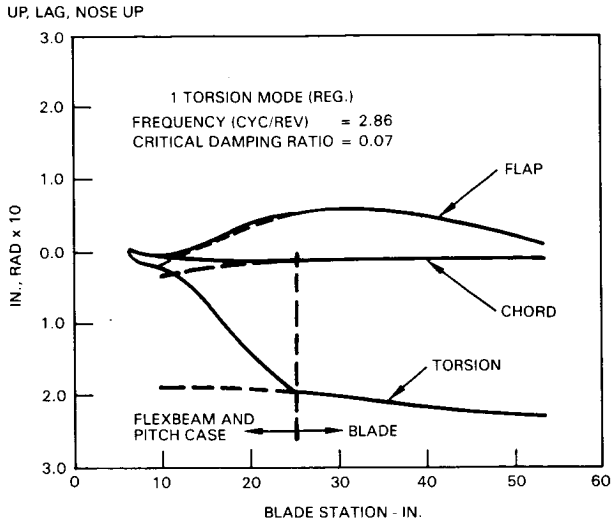

Fig. 31 Cyclic B.C., mode shape plots – 1-torsion mode

This was achieved through placement of the reactionless 1-chord frequency below 1/rev. Comparisons of harmonic loads between the CFTR and a similar size rotor (Reference 12) based on test data are seen in Figs. 32 through 35. Figs. 32 and 33 are flight test loads of the YUH-60A tail rotor. Figs. 34 and 35 are wind tunnel test loads for the CFTR. This comparison is a study of the relative magnitudes of the harmonic loads for geometrically similar rotors with different dynamic characteristics. Absolute magnitudes of the loads should not be compared. The spanwise distribution and relative harmonic content of flapwise flexbeam loads are similar between the two rotors (Figs. 32 and 34). However harmonic contents of chordwise loads between the two rotors are quite different. In Fig. 33 (stiff inplane rotor), chordwise 2/rev loads are higher than the 1/rev loads. The CFTR (Fig. 35, soft inplane rotor) chordwise 2/rev loads are an order of magnitude lower than the 1/rev loads. This trend has been found for all test conditions.

5.1.3 Collective Boundary Condition

The difference between the collective and reactionless boundary conditions are in the model for the control system and drive system. The drive system torsional flexibility is represented by its flexibility in the blade inplane structural model at the hub. The control system stiffness is reflected by the structure from the tail rotor actuators to the pitch horn. The effective mass of the swashplate assembly has a significant influence on the first torsion frequency.

The resonance diagram for the collective boundary condition is shown in Fig. 21 for zero collective pitch. The predicted first chord modal frequency, which is essentially the drive system torsion mode, is omitted in the plot. This is because the frequency and damping of the first chord mode is more accurately predicted in the stability analysis of the tail rotor drive system rather than from the rotor model. The drop in the frequency of the first torsion mode (from those of the reactionless boundary condition) is a reflection of the reduction of control system stiffness and the inclusion of swashplate assembly inertia for the collective boundary condition. The second chord frequency is also reduced as a result of torsional flexibility of the drive system. Experimentally determined 1-chord frequency is included for comparison.

5.2 Harmonic Loads

As discussed in Section 3.0, the CFTR was designed for low chordwise 2/rev Coriolis load.

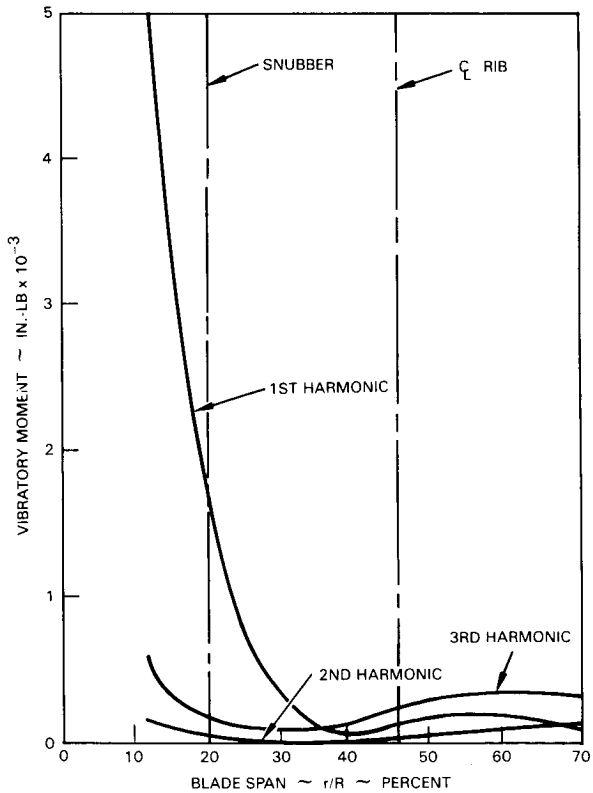

Fig. 32. YUH-60A tail rotor blade harmonic analysis flatwise (V = 143 KTS)

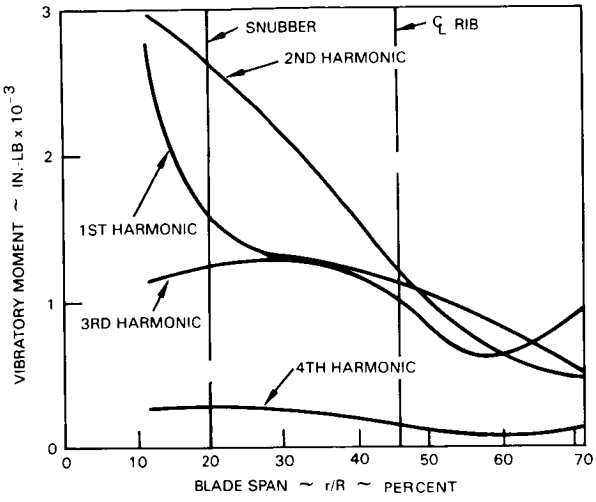

Fig. 33 YUH-60A tail rotor blade harmonic analysis edgewise (V = 143 KTS)

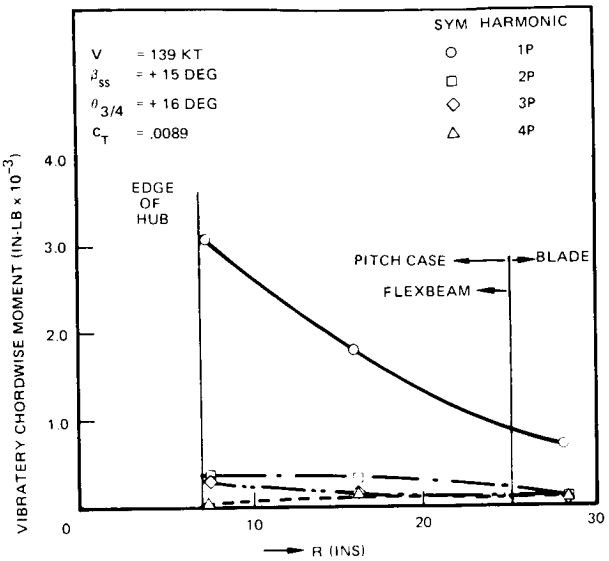

Fig. 35 CFTR - flexbeam harmonic loads

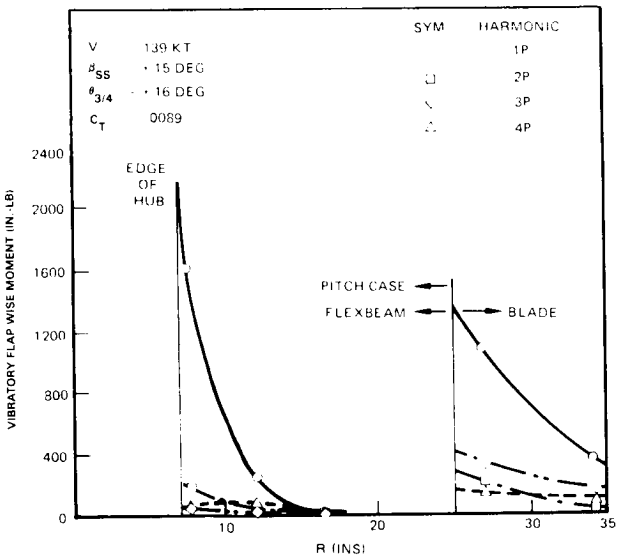

Fig. 34 CFTR - flexbeam harmonic loads

6.0 Concluding Remarks

As discussed in the preceding sections, the HHI Composite Flexbeam Tail Rotor has a dynamically unique design. This rotor has been demonstrated, through wind tunnel tests, over the full sideslip envelope of the AH-64, Advanced Attack Helicopter. The wind tunnel tests have validated that the CFTR:

1) Is aeroelastically stable throughout the complete collective pitch range and up to operational rotor speed of 1403 RPM.

2) Is aeroelastically stable for forward flight speeds up to 197 knots and sideslip flight representative of the AH-64 flight envelope.

3) Has excellent dynamic characteristics at all pitch angles, rotor speeds and test conditions.

4) Exhibits low flexbeam flapwise and chordwise steady and alternating stresses. Loads were well below endurance limit for all conditions tested in the wind tunnel.

5) Does not require a complicated flexbeam cross-section design with elastomeric material sandwiched in the flexbeam to provide damping.

These excellent characteristics have been achieved through judicious choice of design innovations which are the result of industry experience with bearingless rotors. Some of these innovations are discussed below:

1) In order to avoid stability problem characteristics of bearingless tail rotors, the first inplane reactionless (S-mode) frequency was tuned below 1/rev while maintaining the first inplane cyclic (C-mode) frequency above 1/rev. Both frequencies are well separated from the first flap frequency. This was accomplished through the design of the chordwise stiffness of the flexbeam, and by elastomerically mounting the flexbeam to the hub.

2) By allowing the flexbeam to freely flex within the hub, the load transfer to the hub is minimized. The 1/rev chordwise load is maintained within the flexbeam and not transferred to the hub. The 2/rev chordwise loads are transferred to the hub after significant attenuation due

to hub shear pad damping and separation of the first chord reactionless frequency from 2/rev.

3) The trailing edge pitch link attachment was found to be advantageous over a leading edge configuration (for a bearingless rotor of the "pusher" type).

a) For the required kinematic pitch-flap coupling of -35 degrees, the trailing edge pitch link attachment permits a smaller swash-plate and a compact control system design.

b) The trailing edge pitch link attachment raises the second flap frequency, thus providing good separation from 3/rev.

c) The nominal pitch link load (compression) for a trailing edge pitch link attachment is in the same direction as the rotor thrust, thus reducing considerably the flap shear load in the flexbeam, inboard of the pitch shear support.

4) The inclination of the pitch link introduces positive pitch-lag coupling (nose down with blade lag). This coupling adds damping to the first chord cyclic mode through pitch coupling, especially at high collective pitch settings.

5) The relative pitch orientation of the flexbeam chord with respect to the blade chord causes the cyclic first chord frequency to first increase and then decrease through the collective pitch range of the rotor. This ensures minimum decrease of the cyclic first chord frequency and prevents coalescence with the first flap frequency.

6) The above means of introducing damping and of preventing dynamic instabilities involving the lowly damped 1-chord mode, eliminates the need for introducing structural damping through elastomeric inserts in the flexbeam.

7) The leading edge balance weight between station 39 and 51 was introduced to move the blade dynamic center of gravity forward and eliminate blade flutter due to structural failure of the feathering control system.

8) The blade spanwise balance weight is located at station 9.7 (on top and bottom of pitch case) rather than at blade tip. Elimination of tip balance weight increases the cyclic first chord frequency and avoids coalescence with the first flap frequency. The balance weights on the top and bottom surfaces of the pitch case act as "Chinese" weights, thus reducing feathering control loads.

7.0 References

1. Edwards, W.T. and Miao, W., "Bearingless Tail Rotor Loads and Stability", Boeing-Vertol Company, prepared for Applied Technology Laboratory, Research and Technology Laboratories (AVRADCOM), Fort Eustis, VA 23604, USAAMRDL TR 76-16, November 1977.

2. Fenaughty, R.R. and Noehren, W.L., "Composite Bearingless Tail Rotor for UTTAS", Journal of the American Helicopter Society, July 1977.

3. Cook, C.V., A Review of Tail Rotor Design and Performance, Vertica, Vol. 2, pp. 163-181, 1979.

4. Hughes, C.W., "Design and Testing of a New Generation Tail Rotor", Bell Helicopter Textron, presented to the AHS Technical Council for consideration of the Robert L. Lichten Award, February 1978.

5. Maloney, P.F. and Porterfield, J.D., Elastic Pitch Beam Tail Rotor, Kaman Aerospace Corporation, USAAMRDL TR 76-35, U.S. Army Air Mobility Research and Development Laboratory, Fort Eustis, VA 23604, December 1976.

6. Gaffey, T.M., "The Effect of Positive Pitch-Flap Coupling (Negative δ_3) on Rotor Blade Motion Stability and Flapping", Journal of American Helicopter Society, April 1969.

7. Ormiston, R.A. and Hodges, D.H., "Linear Flap-Lag Dynamics of Hingeless Rotor Blades in Hover", Journal of American Helicopter Society 17 (2), April 1972.

8. Head, R.E. and Banerjee, D., "Helicopter Tail Rotor of the Elastomerically-Mounted Composite Flexbeam Type", Patent No. 4,381,902, May 1983.

9. Banerjee, D., "Composite Flexbeam Tail Rotor for the AH-64 Advanced Attack Helicopter Wind Tunnel Test Report", Hughes Helicopters, Inc., Report No. 150-V-2003, HHI 82-362, December 1982.

10. Systems Specification for Advanced Attack Helicopter, AMC-SS-AAH-H10000A.

11. Banerjee, D., "Composite Flexbeam Tail Rotor for the YAH-64 Advanced Attack Helicopter, Aeroelasticity and Rotor Blade Loads Report", Hughes Helicopters, Inc., Report No. 150-V-2001, HHI 82-186, June 1982.

12. YUH-60A - Structural Load Survey, Sikorsky Aircraft Report No. SER-70406.

13. Huber, H., Frommlet, H., and Buchs, W., "Development of a Bearingless Helicopter Tail Rotor", Sixth European Rotorcraft and Powered Lift Aircraft Forum, Paper No. 16, September 16-18, 1980, Bristol, England.